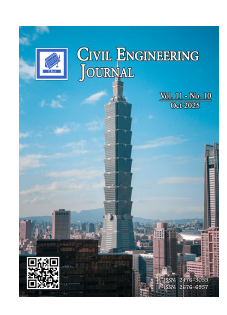


# **Civil Engineering Journal**

(E-ISSN: 2476-3055; ISSN: 2676-6957)

Vol. 11, No. 10, October, 2025



## Recycled Steel Fiber-Reinforced Mortar with Embedded Structural Health Monitoring for Sustainable Construction

Umar Amjad <sup>1\*</sup>, Mohammad R. Irshidat <sup>1\*</sup>, Muni R. Maurya <sup>1</sup>, Naeem Albeitjali <sup>1</sup>, Riyamol K. Razack <sup>1</sup>, Hashem Y. Kailani <sup>1, 2</sup>, Kishor K. Sadasivuni <sup>1</sup>

<sup>1</sup> Center for Advanced Materials (CAM), Qatar University, P.O. Box 2713, Doha, Qatar.

Received 08 July 2025; Revised 16 September 2025; Accepted 21 September 2025; Published 01 October 2025

#### **Abstract**

The study examines the mechanical and microstructural performance of eco-friendly mortar mixes that incorporate Recycled Steel Fibers (RSF) derived from waste tires. Four mortar formulations with varying RSF content (0%, 0.5%, 1%, and 1.5%) by volume) were evaluated for compressive strength, flexural strength, and electrical conductivity. Experimental results revealed that a 1.5% RSF mixture exhibited remarkable improvements in flexural strength, achieving a 67% increase compared to the control formulation while delivering a 12.6% enhancement in compressive strength. However, the 0.5% RSF mix showed reduced performance due to poor fiber dispersion, underscoring the importance of proper fiber distribution. Specific resistance decreased with RSF addition, indicating enhanced electrical conductivity, with the lowest specific resistance observed at 0.5% RSF on day 28. An empirical model using a fiber reinforcing index ( $\xi$ ) was developed to predict strength behavior. A quadratic relationship was found to best describe compressive strength gains, while a linear model effectively captured the flexural strength trend. The models were calibrated using both experimental data and literature values, achieving high predictive accuracy. Electrical conductivity increased with RSF addition, and the slope of the specific resistance during loading correlated strongly with mechanical strength, highlighting its potential as a non-destructive structural health monitoring (SHM) indicator. SEM analysis confirmed improved matrix integrity and fiber-matrix interaction at the optimal 1% RSF content, which balanced strength gains and sensing capability. The study establishes RSF as a viable sustainable alternative to virgin steel fibers, providing both mechanical enhancements and self-sensing properties. This novel integration of electrical monitoring with mechanical testing and modeling provides new insights into recycledfiber composites by enabling simultaneous enhancement of structural performance and real-time damage monitoring.

Keywords: Recycled Steel Fibers (RSF); Cementitious Composites; Mechanical Properties; Sustainable Construction; Fiber Reinforcing Index; Structural Health Monitoring.

#### 1. Introduction

Recent studies have rigorously investigated the integration of recycled materials-including construction and demolition waste, recycled aggregates, and recycled fibers-into concrete and other construction materials, demonstrating their viability for sustainable structural applications without compromising performance [1–3]. Additional studies have confirmed the viability of these sustainable materials in structural applications [4–6]. The use of recycled steel fibers (RSF) derived from waste tires as reinforcement in construction materials, particularly mortar and concrete, has gained substantial attention in recent years due to its potential to improve mechanical properties, enhance durability, and provide significant environmental benefits. Mechanically, RSF has been shown to significantly enhance the tensile, flexural, and

<sup>\*</sup> Corresponding author: umaramjad@qu.edu.qa; mirshidat@qu.edu.qa





© 2025 by the authors. Licensee C.E.J, Tehran, Iran. This article is an open access article distributed under the terms and conditions of the Creative Commons Attribution (CC-BY) license (http://creativecommons.org/licenses/by/4.0/).

<sup>&</sup>lt;sup>2</sup> Department of Civil and Environmental Engineering, Qatar University, PO Box 2713, Doha, Qatar.

shear strengths of concrete, primarily through its crack-bridging capability and its ability to redistribute stress after cracking [7–9]. Multiple studies have reported similar improvements under varied mix designs and test setups [10, 11]. Early work by Aiello et al. [12] established that RSF improves pull-out behavior, compressive strength, and flexural capacity, with experimental results indicating a toughness increase of up to 30% compared to unreinforced concrete, attributed to the fibers' high tensile strength (typically exceeding 1000 MPa) and irregular geometry. This was further confirmed by Centonze et al. [13], who conducted a comprehensive mechanical characterization, reporting that RSF-reinforced concrete exhibits enhanced energy absorption and ductility, with flexural strength improvements ranging from 15% to 25% depending on fiber volume fraction and mix design.

Liew & Akbar [14] provided a thorough overview of recent advancements, noting that RSF's performance rivals that of industrial steel fibers, with post-cracking behavior improved by 20-40% due to its capability to arrest crack propagation. Zia et al. [15] performed a review, discovering that RSF increases split tensile strength by 10-40%, with optimal performance linked to fiber lengths (20-50 mm) and aspect ratios (50-80), although higher proportions can affect workability due to fiber balling. Zhang et al. [16] confirmed these findings, reporting a slight compressive strength increase (5-15%), but notable tensile enhancements (20-35%), emphasizing the importance of fiber-matrix bonding in load transfer. Barros et al. [17] evaluated RSF's potential in cement-based materials, concluding that a fiber volume fraction of 0.5-1.5% maximizes mechanical benefits, with higher content leading to decreased workability and matrix disruption. Amin et al. [18] reiterated this, highlighting that RSF's irregular surface texture enhances interfacial bonding, increasing flexural toughness by 25-30%. Alsaif & Alharbi [19] examined RSF in rubberized concrete, noting a 15-20% increase in tensile strength and a 50% reduction in crack width, along with enhanced shrinkage resistance due to the fibers' stress redistribution capabilities.

Mehmandari et al. [20] focused on split tensile behavior, finding that RSF increases tensile strength by 20-30% and reduces brittle failure, with performance comparable to industrial fibers at lower costs. Meddah & Bencheikh [21] studied various industrial waste fibers, including RSF, reporting shear capacity improvements of 25-35%, which can be attributed to the fibers' random orientation and high tensile strength. Samarakoon et al. [22] indicated similar shear enhancements, with RSF-reinforced concrete displaying a 30% increase in energy dissipation under shear loading. Researchers [23–25] highlighted that RSF's technical potential is maximized at fiber fractions of 1-2%, beyond which gains in flexural toughness diminish due to matrix congestion. Soulioti et al. [26] investigated the effect of fiber volume fraction on flexural behavior, observing a 20-40% increase in flexural strength at 1% RSF, with diminishing returns at higher fractions due to fiber clustering. Centonze et al. [27] examined RSF in lightweight concrete, noting a 20-30% increase in ductility, while Papakonstantinou & Tobolski [28] discovered that steel beads from tires improve compressive strength by 10-15% in Portland cement concrete. Zeybek et al. [29] evaluated RSF's performance under various loading conditions, reporting a 40% increase in energy absorption under impact, while Chen et al. [30] confirmed improvements in dynamic compressive strength of 30-50% under high-strain-rate loading, attributed to RSF's effective energy dissipation capability.

Beyond mechanical enhancements, RSF significantly enhances the durability of concrete, particularly in aggressive environments such as those with chloride exposure, freeze-thaw cycles, and sulfate attack. Frazão et al. [31] investigated RSF's durability in chloride environments, finding that it decreases corrosion rates by 15-20% compared to plain concrete due to its crack-bridging effect, which limits chloride ingress. Carrillo et al. [11] compared industrial and recycled fibers, reporting that RSF-reinforced concrete retains 10-15% greater residual strength after freeze-thaw cycles, with improved resistance to microcracking. Revuelta et al. [32] examined drying behavior and residual strength, finding that RSF reduces shrinkage strain by 20-25% and maintains 85-90% of initial strength post-exposure, thus enhancing long-term durability. Qin et al. [33] emphasized RSF's role in environmentally friendly concrete, noting a 20-30% decrease in drying shrinkage and improved resistance to thermal cracking, extending service life by 25-30%. Li et al. [34] explored waste tire fiber-modified concrete, discovering that RSF mitigates thermal degradation, with strength losses limited to 5-10% under elevated temperatures compared to 15-20% in plain concrete. Mastali & Dalvand [35] investigated hybrid RSF-polypropylene fiber mixes in self-compacting concrete, reporting a 30% reduction in thermal cracking and enhanced fresh-state properties, such as reduced segregation.

Martinelli et al. [36] studied post-cracking behavior in hybrid industrial/recycled fiber mixes, finding that RSF boosts durability by reducing crack propagation rates by 20-25%, particularly under sustained loading. Pilakoutas et al. [37] highlighted RSF's capability to maintain structural integrity in aggressive environments, with permeability reduced by 20-30% due to its crack-arresting properties. Albano et al. [38] examined rubberized concrete with RSF, noting a 10-15% improvement in sulfate resistance, with compressive strength losses limited to 5-10% versus 15-20% in unreinforced mixes. Rashid & Balouch [39] focused on shear behavior in high-strength concrete, finding that RSF enhances durability by decreasing shear crack widths by 30-40%, improving resistance to environmental degradation. Caggiano et al. [40] characterized post-cracking responses in hybrid fiber-reinforced concrete, reporting a 20-30% reduction in water permeability, which enhances resistance to chloride and sulfate ingress. Majeed Abed et al. [41] demonstrated that substituting up to 0.6% RSF in roller-compacted concrete markedly improves toughness and reduces chloride penetration, albeit with minor fresh-density fluctuations. Comparable gains were reported for ultra-

high-performance concretes, where hybrid RSF-industrial fibers sustain compressive strengths above 130 MPa while lowering embodied carbon [42]. Experimental campaigns on alkali-activated and slag-based mixes show that RSF dosages of 0.5-1% restore or exceed the splitting- and flexural-tensile capacity forfeited when rubber aggregates are introduced, with hybrid RSF/deformed fibers yielding the highest toughness indices [43]. At elevated temperatures, RSF-reinforced concretes retain up to 40% more residual compressive strength than plain mixes, a benefit linked to the fibers' crack-bridging efficacy and verified by reduced mass loss and denser micro-structures in Scanning Electron Microscopy (SEM) analysis [44].

Environmentally, RSF offers a sustainable alternative to traditional reinforcement materials by repurposing waste tires, reducing landfill burdens, and lowering the carbon footprint of concrete production. Pilakoutas et al. [37] estimated that recycling tire steel fibers could divert millions of tons of waste annually, reducing landfill use by 10-15% in tire-heavy regions, while also cutting raw material extraction by 20-30%. Qin et al. [33] quantified environmental benefits, reporting that RSF production emits 50-70% less CO<sub>2</sub> than industrial steel fiber manufacturing, offering a low-carbon alternative with energy savings of 30-40%. Frazão et al. [45] highlighted that RSF reduces the environmental impact of concrete by 25-35%, aligning with circular economy principles through waste valorization. Zia et al. [15] and Zeybek et al. [29] emphasized that RSF minimizes the need for virgin steel, reducing energy consumption by 30-40% and mitigating the environmental degradation associated with mining and steel production. However, challenges persist, including variability in RSF quality (e.g., residual rubber content), which can affect consistency and long-term performance [13, 18]. Workability issues at higher fiber contents (above 2%) and potential corrosion risks in highly aggressive environments are also noted [14, 31]. Despite these limitations, incorporating RSF into construction materials provides an optimal balance of improved mechanical properties, enhanced durability, and environmental benefits, with applications ranging from structural components to pavements and lightweight composites.

Other aspects of the RSF application include its economic feasibility and practical implementation. RSF's low cost (often 50-70% less than industrial fibers) makes it an attractive option for large-scale construction, particularly in developing regions [37]. However, processing challenges, such as separating fibers from rubber and ensuring uniform quality, require further optimization [15]. Mix design adjustments are critical, as RSF's irregular shape can reduce slump and increase mixing time [27]. Hybrid approaches, combining RSF with other fibers (e.g., polypropylene), offer a promising avenue to balance mechanical and fresh-state properties [35, 36, 46]. Moreover, RSF's versatility extends to specialized applications, such as self-compacting concrete [46] and high-strength concrete; however, further research is needed to standardize RSF usage and address scalability challenges.

However, relatively few studies have simultaneously explored RSF's role in enhancing mechanical performance and enabling self-sensing (for structural health monitoring), nor have they developed empirical models that incorporate fiber geometry and content to predict composite behavior. Consequently, important knowledge gaps remain in harnessing RSF's full potential for smart and sustainable infrastructure. This study addresses these gaps by adopting a novel integrated experimental—empirical approach. Electrical conductivity measurements (to evaluate self-sensing behavior) are combined with conventional mechanical testing and an empirical fiber reinforcing index model, providing a comprehensive assessment of RSF's effects. This approach distinguishes the present work from prior research by enabling concurrent evaluation of structural performance improvements and real-time damage monitoring. In short, the present study evaluates RSF's impact on mechanical strength and durability, investigates its self-sensing capability for damage detection, and develops a predictive strength model using a fiber reinforcing index, thereby filling critical gaps in existing literature.

The manuscript is organized as follows: Section 2 describes the experimental procedure, including materials, mix design, and test methods. Section 3 presents and discusses the results: compressive and flexural behavior, electrical specific resistance and percolation, the empirical model based on the fiber-reinforcing index, and SEM observations. Section 4 concludes with findings and implications for sustainable construction material.

#### 2. Experimental Program

In this experimental program, a combined approach was utilized, integrating conventional mechanical testing with real-time electrical resistance measurements to evaluate both the structural performance and self-sensing behavior of RSF-reinforced mortars.

### 2.1. Mix Design and Materials Properties

Mixing design plays a critical role in the development of eco-friendly mortars with improved performance characteristics. To ensure practical applicability, the mixture must satisfy the specific strength and durability criteria while maintaining adequate workability for ease of placement and consolidation. Four RSF loading levels, i.e., 0%, 0.5%, 1%, and 1.5% by volume, were investigated to assess their influence on mortar properties. The RSF, procured in bulk quantities, was sourced from three randomly selected batches (A, B, and C) to simulate real-world material variability, with fibers from batches A, B, and C assigned to 0.5%, 1%, and 1.5% mixtures, respectively. As specified

by the supplier, the RSF dimensions ranged from 0.2 to 0.3 mm in diameter and 10 to 60 mm in length. A constant water-to-binder (W/B) ratio of 0.5 and binder-to-sand (B/S) ratio of 1:2 [47] was maintained across all mixtures to ensure comparable workability and facilitate a direct assessment of the influence of the RSF [48]. Mortar preparation, casting, and curing were performed according to the ASTM standards to ensure experimental consistency. Following ASTM C305-13 [49] guidelines, mortar mixtures were prepared using a standard mechanical mixer. The dry components, including the cement and sand, are dry-mixed for one minute to achieve homogeneity. Water was then gradually introduced while mixing continued for an additional three minutes, ensuring a uniform constituent distribution within the mortar matrix. Fresh mortar was cast into standard molds (cubic: 50 mm  $\times$  50 mm  $\times$  50 mm and prisms: 40 mm  $\times$  40 mm  $\times$  160 mm) according to the ASTM test method (ASTM C109/C109M-20b [50] for compressive strength and ASTM C348-21 [51] for flexural strength). Curing was performed in a temperature-controlled water bath maintained at 23  $\pm$  2°C to promote consistent cement hydration and minimize strength variability. This study used Type II Portland Cement, conforming to ASTM C150/C150M-22 [52]. The chemical composition of the cement, including its major constituents, is presented in Table 1. To meet the requirements for fine aggregates, locally sourced silica sand conforming to the ASTM C778-13 [53] standards was incorporated into the mixture design.

Compound	%
CaO	56.02
${ m SiO_2}$	24.59
$Al_2O_3$	5.87
$Fe_2O_3$	4.67
MgO	2.87
$SO_3$	2.49
$Na_2O$	0.55
$K_2O$	0.58
Loss on ignition	0.80

Table 1. Chemical compositions of Type II Portland cement used in the study

Table 2 presents the detailed mix designs for control mortar and RSF-modified mortars. The control mix served as a baseline for evaluating the changes in properties induced by RSF incorporation. Fine sand served as the primary aggregate in all the mixtures.

Mix design	Cement (g)	RSF (g)	Fine Sand (g)	Water (g)
Control (0% RSF)	850	0	1700	425
0.5% RSF	850	53	1700	425
1% RSF	850	105	1700	425
1.5% RSF	850	157	1700	425

Table 2. Mix Design used in the study

## 2.2. Characterization and Test Procedures

The surface morphologies of the mortar mixes were examined using a benchtop SEM (JEOL JCM-6000). The compressive and flexural strength tests of the prepared mortar mixes were performed using a universal testing machine according to ASTM C109/C109M-20b [50] and ASTM C348-21 [51], respectively. The schematic representing the methodology adopted in the present study is shown in Figure 1. The electrical conductivity of the mortar mixes was estimated by measuring the resistance with a Keithley 2400 source measuring unit (SMU) under a DC bias of 5V. To estimate the electrical conductivity, a prism block of mortar mixed with dimensions of 40 mm  $\times$  40 mm  $\times$  160 mm was prepared. Two copper electrodes with a thickness of  $0.2 \pm 0.01$  mm, a width of  $2 \pm 0.2$  cm and a length of  $4 \pm 0.2$  cm were embedded in the specimen (six samples per mix design) during the molding process. The average depth of electrode inside the specimen, and distance between the electrodes were  $2.5 \pm 0.2$  cm and  $4 \pm 0.2$  cm, respectively. The conductivity of the sample was determined by measuring its resistance during curing. During the flexural strength tests, these embedded electrodes were connected to the Keithley 2400 SMU to continuously monitor the specimen's electrical resistance in real-time. The resistance data were recorded simultaneously as load was applied, enabling correlation between crack formation and changes in electrical response. The specific resistance was used to analyze the conductivity and was calculated using Equation 1.

$$\rho = R \frac{A}{L} \tag{1}$$

where R is the measured resistance, A is the average contact area of the electrode with the mix, and L is the average distance between electrodes.

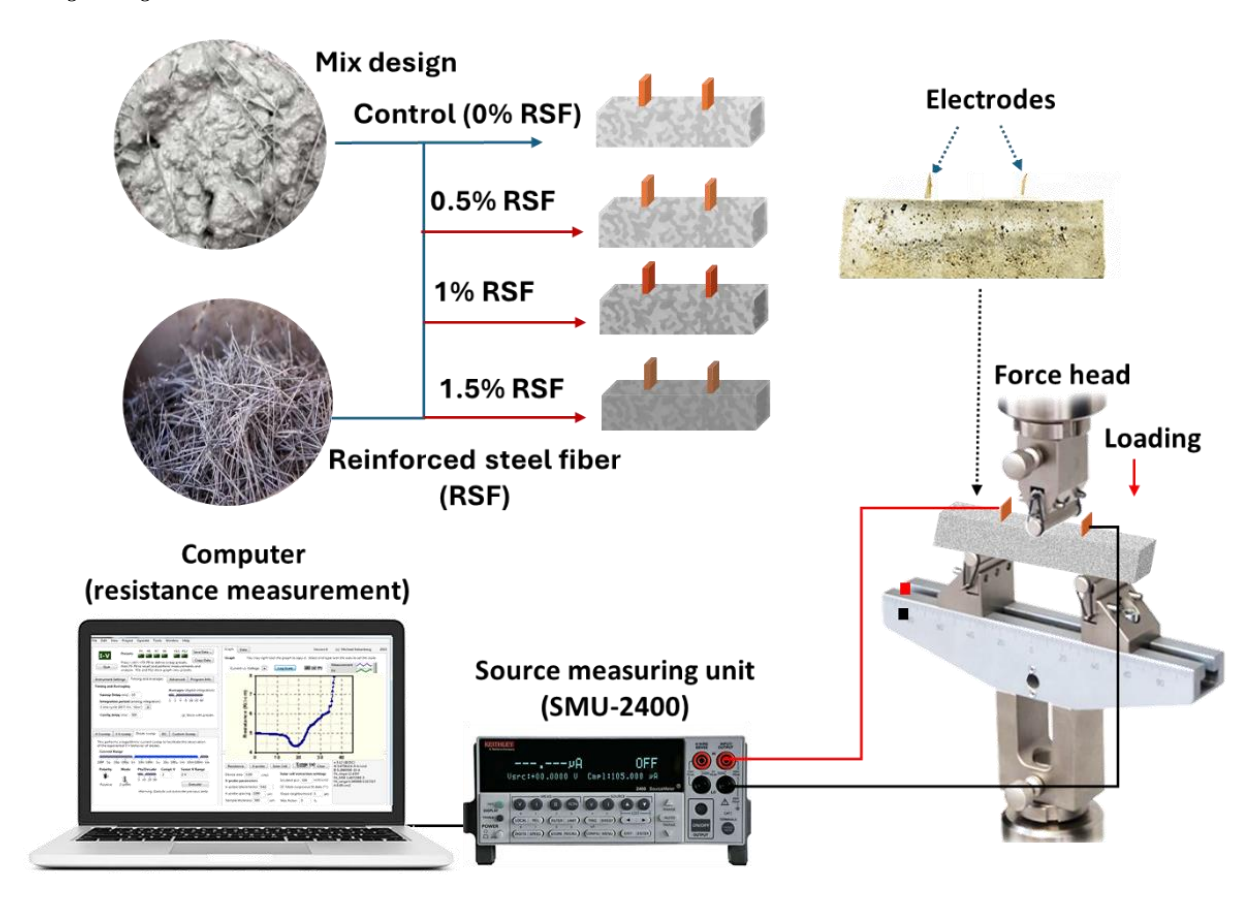


Figure 1. Schematic represents the methodology of the study

## 3. Results and Discussion

#### 3.1. Compressive Strength Analysis

Figure 2-a presents a schematic illustrating the compressive strength test setup and an image of the sample used for the compressive test. The tests were conducted on mortar cube samples (six samples per mix design) with dimensions of 50 mm  $\times$  50 mm  $\times$  50 mm. Figure 2-b shows the variation in average compressive strength of mortar samples with increasing RSF content at curing times of 3 days and 28 days. The obtained compressive strength data are presented in Table 3. On day 3, the compressive strength demonstrates a non-linear trend. The control sample (0% RSF) recorded a strength of 11.90 MPa. The 0.5% RSF mix dropped to 9.90 MPa, suggesting that even a small fiber addition can weaken the matrix if the fibers are not well dispersed, potentially creating voids or zones of stress concentration.

This counterintuitive drop highlights the importance of uniform fiber distribution, i.e., poorly dispersed fibers can act as flaws in the matrix rather than as reinforcement. Both the 1% and 1.5% RSF mixes exhibited significant increases to 14.95 MPa and 14.96 MPa, respectively, highlighting the beneficial effects of RSF in bridging microcracks and enhancing early-age strength. On day 28, the control reached 44.45 MPa, while the 0.5% RSF sample lagged at 29.76 MPa, reinforcing the earlier concern about suboptimal fiber distribution. Compressive strength appears to peak around the 1–1.5% RSF range. The mix with 1% RSF achieved a modest 7% strength gain over the control, while 1.5% RSF provided a slightly higher 12% increase; however, this fell within the data scatter, indicating no statistically significant improvement beyond about 1% fiber content. Excessive fibers may disrupt the composite's homogeneity, emphasizing that incremental additions do not proportionally improve performance. The results highlight 1% RSF as a practical threshold for maximizing benefits while maintaining structural consistency.

Table 3. Average compressive strength of day 3 and day 28 samples with respect to the increase in RSF loading

Day	0% RSF (MPa)	0.5% RSF (MPa)	1% RSF (MPa)	1.5% RSF (MPa)
3	$11.90\pm0.81$	$9.90 \pm 0.50$	$14.95 \pm 1.21$	$14.96 \pm 0.79$
28	44.45 ±1.53	$29.76 \pm 0.41$	$47.80\pm1.82$	$50.10 \pm 3.50$

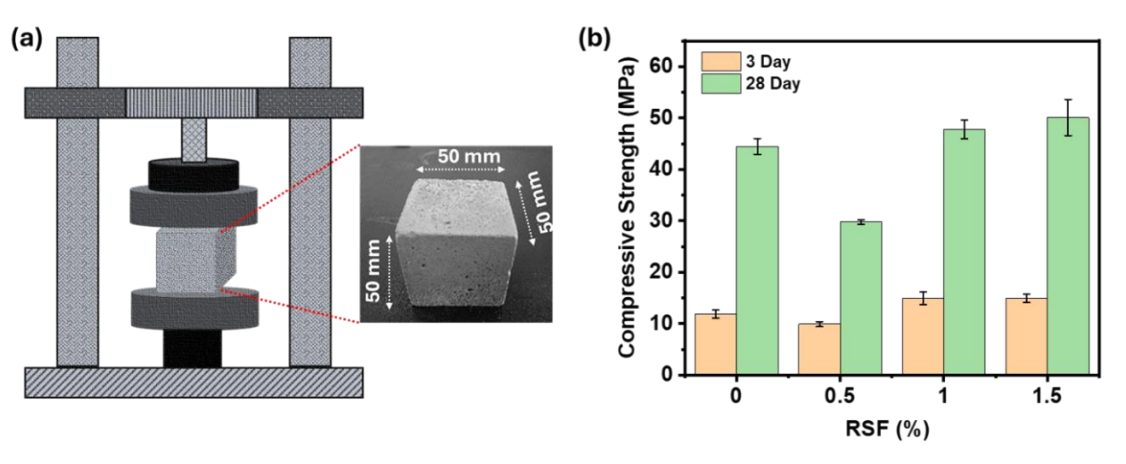


Figure 2. (a) Schematic of compression test setup along with  $50 \times 50 \times 50$  mm sample used for the test; (b) The average compressive strength of the sample with the increase in RSF loading

## 3.2. Flexural Strength Analysis

Flexural strength is a key indicator of a material's capacity to resist bending or deformation under load. Figure 3-a shows a schematic of the testing setup, along with an image of the sample used to assess the flexural strength of the mix. The measurements were performed on prism specimens (six samples per mix design) measuring  $40 \text{ mm} \times 40 \text{ mm} \times 160 \text{ mm}$ . Figure 3-b illustrates the flexural strength development of mortar samples incorporating varying contents of RSF at curing ages of 3 days and 28 days. The flexural strength data is presented in Table 4. At day 3, the flexural strength increases progressively with RSF content. The control mix (0% RSF) recorded flexural strength of 2.98 MPa. Adding 0.5% of RSF slightly improved strength to 3.25 MPa, and 1% RSF further increased it to 3.34 MPa. The 1.5% RSF mix showed a substantial jump to 5.07 MPa, reflecting a 70% increase over the control.

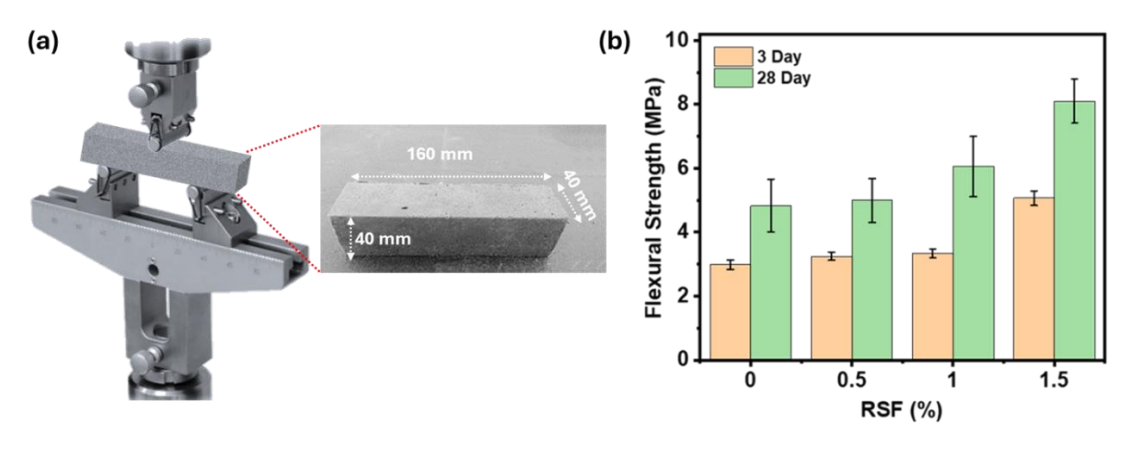


Figure 3. (a) Schematic of flexural test setup along with a image of  $40 \times 40 \times 160$  mm sample used for the test; (b) Average flexural strength of the sample with the increase in RSF loading

Table 4. Average flexural strength of day 3 and day 28 samples with respect to the increase in RSF loading

Day	0% RSF (MPa)	0.5% RSF (MPa)	1% RSF (MPa)	1.5% RSF (MPa)
3	$2.98 \pm 0.15$	$3.25\pm0.13$	$3.34 \pm 0.14$	$5.07 \pm 0.23$
28	$4.83 \pm 0.83$	$5.00 \pm 0.69$	$6.06 \pm 0.94$	$8.10 \pm 0.69$

On day 28, a trend similar to day 3 was observed; the control mix reached 4.83 MPa, while the 0.5% and 1% RSF mixes increased to 5.00 MPa and 6.06 MPa, respectively. The 1.5% RSF mix achieved the highest flexural strength of 8.10 MPa, representing a 67.6% increase compared to the unreinforced mortar. Flexural strength benefits more noticeably from RSF due to the fibers' ability to bridge macrocracks, delay crack propagation, and enhance energy absorption under tensile stress. Flexural strength benefits more noticeably from RSF inclusion due to the fibers ability to bridge macrocracks, delay crack propagation, and enhance energy absorption under tensile stress. Unlike compressive strength which tends to plateau or even decline at high fiber contents, flexural strength continued to rise almost linearly up to 1.5% RSF. The greater ductility observed at higher fiber doses confirms that the fibers effectively bridge cracks under bending, delaying fracture and enhancing post-crack load-bearing capacity. The increased ductility and toughness at higher RSF contents confirm that the fibers actively engage during bending, resisting fracture and improving post-crack behavior.

#### 3.3. Specific Resistance Analysis

Figure 4 presents the variation in specific electrical resistance of mortar samples with increasing RSF content, measured at 3 and 28 days of curing. The corresponding specific resistance data is presented in Table 5. On day 3, the control sample (0% RSF) has the highest specific resistance of 1145.43  $\Omega$ ·cm. With 0.5% RSF, specific resistance drops significantly to 869.15  $\Omega$ ·cm, indicating an improvement in conductivity due to the introduction of conductive steel fibers.

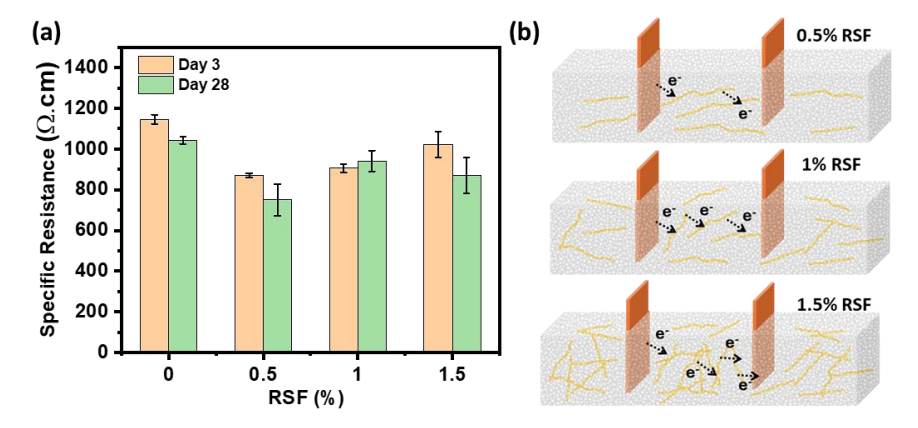


Figure 4. (a) Specific resistance measurement of the sample with the increase in RSF loading; (b) Schematic showing fiber distribution in different volume percentage RSF loaded samples, with a possible charge flow pathway indicated by the black arrow.

Table 5. Specific resistance of day 3 and day 28 samples with an increase in RSF loading

Day	0% RSF (Ω.cm)	0.5% RSF (Ω.cm)	1% RSF (Ω.cm)	1.5% RSF (Ω.cm)
3	$1145.43 \pm 22.68$	$869.15 \pm 10.98$	$905.15 \pm 20.49$	$1022.98 \pm 63.31$
28	$1043.32 \pm 17.45$	$749.57 \pm 77.67$	$941.25 \pm 51.2$	$870.23 \pm 88.7$

At 1% RSF, specific resistance slightly increases to 905.15  $\Omega$ ·cm, suggesting a minor loss of connectivity, possibly due to increased interface resistance with an increase in RSF loading. At 1.5% RSF, specific resistance rises further to 1022.98  $\Omega$  cm, remaining lower than the control, indicating a decline in the efficiency of the conductive network, potentially due to fiber clustering. By day 28, a similar pattern is observed; the control sample measures  $1043.32 \,\Omega \cdot \text{cm}$ . The 0.5% RSF sample again exhibits the lowest specific resistance at 749.57 Ω·cm. A study revealed that the resistance decreases with an increase in the fiber index ratio, which is directly proportional to the volume of the fiber and fiber aspect ratio (AR) (length/diameter) [54]. In the present study, the 0.5% RSF is the lowest volume of fiber added in the sample and exhibits the lowest specific resistance. This indicates the presence of fibers with very large AR that result in the enhancement of conductivity. Specific resistance increases to 941.25 Ω·cm at 1% RSF and slightly decreases to  $870.23 \Omega \cdot \text{cm}$  at 1.5% RSF, but does not drop to the low values noted at 0.5%. Figure 4-b shows the possible conducting pathway for different RSF volume percent-loaded samples. The 0.5% RSF sample achieved the highest conductivity, indicating the presence of high AR fibers with almost horizontal dispersion in the sample. As a result, most of the charge flow pathway is from the fiber and covers less mortar pathway between the electrodes. At 1% RSF, the fiber tends to form efficient conductive bridges. However, due to deviation from the horizontal arrangement, the mean path charges must cover mortar increases, as shown in Figure 4-b. As a result, specific resistance increases for the 1% RSF sample compared to the 0.5% RSF sample. Higher RSF content (1.5% RSF) could lead to fiber clumping and poor alignment that disrupts the conductive pathway. This could further increase the average path length that charges must travel through the mortar, resulting in higher resistance.

The electrical results show a non-linear percolation behavior as fiber content increases. At 28 days, the control mix (0% RSF) exhibits the highest specific resistivity of 1043.32  $\Omega$ ·cm, representing a non-percolating system where only the cement matrix provides conduction. Adding 0.5% RSF drops resistivity sharply to 749.57  $\Omega$ ·cm. This reduction confirms that a continuous conductive network has formed, placing the system near the percolation threshold where adjacent fibers contact to create electrically conductive paths [55].

At 1.0% RSF, resistivity rises to 941.25  $\Omega$ ·cm, and at 1.5% RSF, it reaches 870.23  $\Omega$ ·cm (both remain lower than the control but exceed the 0.5% value). This unexpected increase at higher fiber contents stems from clustering and poor fiber orientation. Once the percolation threshold is exceeded, adding more fibers disrupts the established network (Figure 4-b). At 0.5% RSF, the high AR fibers dispersed well and created efficient conductive pathways. At 1.0% and 1.5% RSF, redundant connections and fiber agglomeration increased the average resistive path length. The measured paste width between adjacent particles decreases as fiber content increases, limiting workability and fiber dispersion effectiveness. This behavior confirms an optimal fiber content exists for electrical percolation in this system, between 0.5% and 1.0%. Above this range, additional fibers fail to reduce resistivity unless they form well-connected networks without excessive clustering [54].

#### 3.4. Empirical Modeling of Strength Parameters Based on Fiber Reinforcing Index

Given the non-linear impact of fiber content observed in empirical studies, particularly concerning compressive strength characteristics, quantitative models were developed to clarify the correlation between fiber dosage and strength parameters. Instead of treating fiber volume fraction and AR as separate variables, a singular composite metric, known as the fiber reinforcing index ( $\xi$ ), was utilized. This approach, originally developed by Ou et al. [56], offers a generalized representation of fiber influence by combining volume fraction and AR into one parameter. It is superior to treating these variables separately because it captures the cumulative reinforcing capacity across varying fiber geometries. The reinforcing index is defined by Equation 2.

$$\xi = \mathbf{v} \times \mathbf{AR} \tag{2}$$

where v denotes the fiber volume fraction and AR signifies the fiber aspect ratio (the ratio of length to diameter). This index encapsulates the cumulative reinforcing capacity of fibers; enhancements in either volume or AR led to elevated  $\xi$  values. The integration of  $\xi$  allows the model to maintain its applicability across diverse fiber classifications and quantities, a methodology that has been substantiated by previous studies linking  $\xi$  with mechanical efficacy.

#### 3.4.1. Model for Compressive Strength

Let  $f_{c0}$  represent the compressive strength of conventional, unreinforced concrete. The incorporation of fibers typically enhances compressive strength at lower quantities by bridging microcracks and inhibiting the progression of cracks. Nevertheless, at elevated quantities, this advantage may wane or even become negative as a result of the emergence of defects, agglomeration, or inadequate fiber-matrix adhesion. To encapsulate this non-linear behavior, a quadratic function of  $\xi$  is proposed in Equation 3.

$$f_c = f_{c0}(1 + a\xi - b\xi^2)$$
 (3)

In this context,  $f_c$  represents the compressive strength of RSF reinforced concrete, the parameter 'a' represents a positive coefficient that denotes the initial enhancement effect attributable to the incorporation of fibers, whereas the parameter 'b' serves as a positive coefficient that accounts for the diminishing efficiency or potential reduction in strength that occurs at elevated fiber concentrations. Thus, the model captures a concave-down behavior: initial fiber inclusion improves strength (a\xi\$) but excessive fiber leads to strength loss ( $-b\xi^2$ ). The peak compressive strength occurs at the optimal reinforcing index:

$$\xi_{\text{opt}} = a/2b \tag{4}$$

This optimal juncture signifies the most efficacious fiber content for the augmentation of compressive strength.

### 3.4.2. Model for Flexural Strength

Flexural strength, referred to as  $f_{flex}$ , exhibits a considerably heightened sensitivity to the incorporation of fibers compared to compressive strength, owing to the pivotal function of fibers in effectively bridging macrocracks and countering tensile failure. Let  $f_{flex0}$  denote the flexural strength of unreinforced concrete. In contrast to the behavior observed under compression, empirical data suggest a nearly linear augmentation in flexural strength corresponding to increased fiber content, particularly within the frequently utilized dosage range (0–1.5% by volume). Therefore, a linear model in terms of  $\xi$  is proposed:

$$f_{flex} = f_{flex0}(1 + c\xi) \tag{5}$$

The coefficient c signifies the effectiveness of fibers in augmenting flexural capacity. Comparable linear associations have been corroborated by antecedent research, including design frameworks such as ACI 544 and contemporary empirical studies [57].

Coefficients a, b, and c will be optimized based on regression analysis of both the current experimental dataset and supplementary data from the literature.

### 3.4.3. Model Calibration and Validation

To obtain representative coefficients a, b, c for the models, we compiled data from multiple published studies on RSF or waste-steel-fiber reinforced concrete, as represented in Table 6. From each data source, we extracted the plain concrete strength ( $f_{c0}$ ,  $f_{flex0}$ ) and the strengths achieved at one or more fiber contents (with known fiber AR). We then calculated  $\xi$  for each fiber case and computed the percentage strength increase (increase in strength divided by plain or control sample strength). Using nonlinear regression (least squares fitting), we solved for the best-fit a, b in Equation 3 and c in Equation 5 that minimize the error between predicted and observed strengths.

Reference	RSF (%)	AR	Compressive strength gain (%)	Flexural strength gain (%)	a	b	c
Aiello et al. [12]	0.5	65	10-15	-	0.615-0.923	0.947-1.42	-
	1.0	65	5	-	0.153	0.118	-
Leone et al. [58]	0.5	65	12	30	0.734	1.136	0.92
Centonze et al. [13]	1.5	80	15	50	0.249	0.104	0.416
Mastali & Dalvand [46]	1.5	50	25	70-75	0.666	0.446	0.933-
arżyński & Suchorzewski [59]	1.0	80	10	30	0.249	0.156	0.37

Table 6. Data from published studies on RSF or waste-steel-fiber reinforced concrete

From these studies, a pattern emerges: compressive gains are modest (0–25%) and tend to peak around 1% fiber, while flexural gains are significant (20–75%) and roughly proportional to fiber volume. Fitting Equation 3 to the compressive data yielded  $a\approx0.5$  and  $b\approx0.40$  as a good average. For example, plugging  $\xi=0.80$  (which is ~1% RSF of AR 80) gives  $1+0.5(0.8)-0.4(0.8)^2=1.144$ , i.e. a +14.4% increase. That aligns with many observations (around 10–15% increase at ~1% fiber). The peak of this model occurs at  $\xi=a/(2b)=0.5/(0.8)=0.625$  (~0.6–0.7 in  $\xi$ ), meaning if AR ~100, an optimum around v=0.6-0.7 fiber. But the decrease beyond that is gradual; at  $\xi=1.2$  (about 1.5% fiber with AR 80) the model gives  $1+0.5(1.2)-0.4(1.2)^2=1.024$  (+2.4%), indicating a plateau by 1.5%. This behavior slight drop-off at high fiber content and matches reports that very high RSF content yields no further compressive gain. For flexural strength, fitting a straight line through the literature data gave  $c\approx0.50$  as an average. This means each  $\xi=1.0$  (e.g. 1% fiber of AR 100) yields about +50% flexural strength. In Leone (2016),  $\xi=0.5\times65=0.325$  gave +30% flexural (our model would predict +16% for that  $\xi$ , underestimating that case slightly). In Mastali (2016),  $\xi=1.5\times50=0.75$  gave +70% (model predicts +37%, underestimating). In our data,  $\xi=0.80$  gave +26% (model +40%, slightly overestimating). These variances suggest scatter in c, but generally 0.50 is in the midrange.

The calibrated coefficients  $a \approx 0.50$ ,  $b \approx 0.40$ ,  $c \approx 0.50$  make the model broadly consistent with both our data and others' results. We will use this model in the discussion to interpret the "optimal" fiber content and compare it to what was observed experimentally.

## 3.4.4. Validation with Experimental Data

We now compare the model predictions to the actual strengths measured in our experiments. Table 7 presents the measured vs. predicted values for our mixes. The baseline strengths used were  $f_{c0} = 44.5$  MPa and  $f_{flex0} = 4.8$  MPa (from our control mix). The coefficients used were a = 0.50, b = 0.40, c = 0.50 as discussed.

Table 7. Predicted vs. experimental strengths for the present study RSF mixes. Predictions use Equation 3 and Equation 5 with a=0.50, b=0.40, c=0.50. The percentage error is calculated as ((Pred. – Exp.)/Exp.)  $\times$  100%

RSF (%)	$f_c$ Exp. (MPa)	f <sub>c</sub> Pred. (MPa)	Error (Comp)	$f_{flex}$ Exp. (MPa)	$f_{flex}$ Pred. (MPa)	Error (Flex)
0	44.5	44.5 (by def.)	0.0%	4.8	4.8 (by def.)	0.0%
0.5	29.8	50.5	+69.4%	5.0	5.7	+14.0%
1	47.8	50.3	+5.2%	6.1	6.7	+9.8%
1.5	50.1	45.5	-9.1%	8.1	7.6	-6.1%

We see that except for the 0.5% compressive case, the model predictions are reasonably close within reasonable error margins ( $\pm 10\%$ ). For specimens containing 1.0% and 1.5% RSF, the compressive strength predictions exhibit errors of  $\pm 5.2\%$  and  $\pm 9.1\%$  respectively, while flexural strength predictions show deviations of  $\pm 9.8\%$  and  $\pm 6.1\%$ . These error magnitudes are well within acceptable limits considering the inherent variability typically observed in cementitious composite testing. Additionally, these errors are quite small considering normal experimental scatter, suggesting the chosen a, b, c are appropriate. The 0.5% RSF compressive result, however, is dramatically under-predicted: the model predicted a gain to  $\pm 50.5$  MPa, whereas the experiment was only  $\pm 29.8$  MPa. This corresponds to a  $\pm 69.4\%$  error, because the model could not foresee the strength drop.

This discrepancy is explained by the fact that the model assumes well-distributed fibers enhancing strength, whereas in reality the 0.5% mix fibers were poorly dispersed and introduced. Essentially, 0.5% data point is an outlier caused by uneven fiber distribution, which the model-assuming uniform fiber effects fails to account for. If we exclude that anomalous point, the model captures the general trend of a slight compressive optimum and linear flexural increase quite well.

#### 3.5. Analyzing Specific Resistance Under Continuous Loading

Figure 5 illustrates the variation in specific resistance of mortar samples with different RSF contents during flexural strength testing at 28 days of curing. The electrical response under mechanical stress reveals how internal cracking and fiber-matrix interactions influence electrical conductivity. For the 0% RSF sample, the current primarily travels through the cement matrix. As cracks develop during initial loading, the lack of bridging or conductive pathways causes minimal change. However, at the breakpoint a sudden surge in specific resistance was noticed, as shown in Figure 5-a. Specific resistance starts to increase slightly during loading for the 0.5% RSF-loaded sample. However, the rate of change is not smooth, likely due to less number of fibers supporting the fracture of the specimen, as shown in Figure 5-b. For the 1% RSF sample, specific resistance increases gradually as cracks propagate. At breaking, the curve is smoother, indicating better fiber distribution and bonding, which maintains conductivity even as damage initiates, as shown in Figure 5-c. A stable and gradual rise in specific resistance of a 1% RSF sample reflects good fiber-matrix bonding, indicating a healthy mechanical profile.

The 1.5% RSF sample shows an accelerated increase in specific resistance compared to other samples during flexural loading, suggesting extensive fiber engagement (see Figure 5-d). The real-time resistance changes correlate with crack initiation and propagation during flexural testing. As cracks form and widen, the conductive fiber network is disrupted, leading to rising specific resistance. By analyzing the slope and pattern of this change, it is possible to estimate the damage level in the material. For instance, a steep slope indicates rapid loss of conductive pathways (as seen in the poorly dispersed 0.5% RSF case), whereas a gentle slope (as in the well-dispersed 1% RSF case) indicates gradual damage accumulation. By combining continuous electrical monitoring with microstructural validation, a non-destructive real-time sensing approach can be developed to predict and assess structural integrity, which is especially useful for smart infrastructure applications.

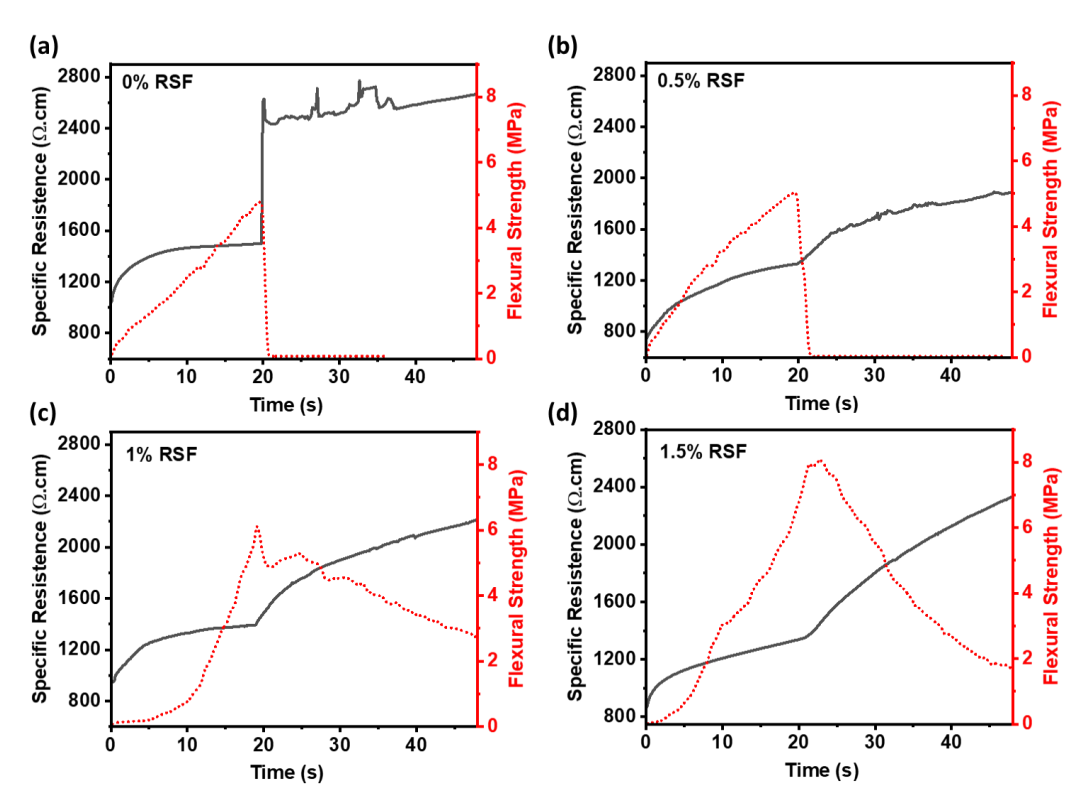


Figure 5. Graphs represent a change in specific resistance with a change in load during flexural strength test for 28-day cured mix sample (a) 0% RSF loaded sample; (b) 0.5% RSF loaded sample; (c) 1% RSF loaded sample; (d) 1.5% RSF loaded sample

Figure 6 shows the change in specific electrical resistance during flexural loading for mortar samples with varying RSF content (0%, 0.5%, 1%, and 1.5%), along with a picture of the sample after the flexural test. The specific resistance response is analyzed after 5 s from the onset of loading to the point of break initiation, and the region of each curve is linearly fitted to quantify the slope, representing the rate of specific resistance increase during crack propagation. The linear fit to the control (0% RSF) sample exhibits the lowest slope of 5.36 with R<sup>2</sup> of 0.865, as shown in Figure 6-a. The change in specific resistance is slow compared to other samples, indicating minimal conductive pathways and poor crack bridging. The 0.5% RSF sample displays the highest slope of 18.91

in the fitted region with R<sup>2</sup> of 0.967, as shown in Figure 6-b. However, this is not indicative of superior performance. Rather, the abrupt and unstable resistance rise is attributed to poor dispersion and weak bonding of the fibers with the mortar. The insufficient and unevenly distributed RSF results in erratic conduction behavior, inconsistent crack bridging, and premature failure. Compared to the control sample, the 1% RSF and 1.5% RSF samples show a progressive increase in the slopes in the fitted linear segment.

The 1% RSF sample slope was estimated to be 9.46, with  $R^2$  of 0.944 (Figure 6-c), and the 1.5% RSF sample linear fitting slope was 13.73, with  $R^2$  of 0.997 (Figure 6-d). An improvement in the linear fitting was observed, indicated by the improvement in  $R^2$  value with an increase in RSF loading. The smooth, gradual slope observed in the 1% and 1.5% RSF samples reflects robust fiber engagement and effective stress transfer across microcracks. The distributed RSF in 1% and 1.5% RSF samples forms a more continuous conductive network, leading to a smoother, more gradual rise in resistance. This suggests more effective crack propagation bridging due to improved fiber-matrix bonding.

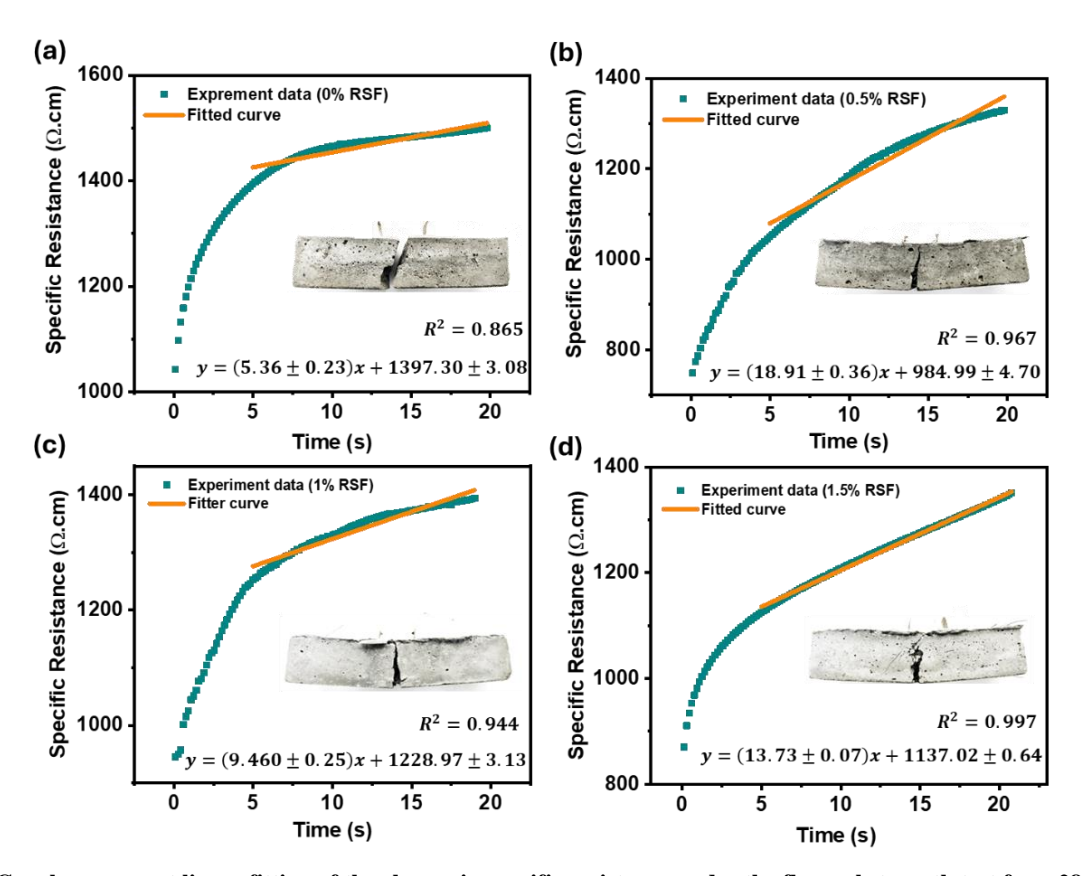


Figure 6. Graphs represent linear fitting of the change in specific resistance under the flexural strength test for a 28-day cured mix sample. (a) 0% RSF loaded sample; (b) 0.5% RSF loaded sample; (c) 1% RSF loaded sample; (d) 1.5% RSF loaded sample.

Experimental analysis of RSF-reinforced mortars across the 0.5%, 1.0%, and 1.5% dosage groups revealed critical relationships between fiber geometry, dispersion quality, and mechanical performance, with batch-specific manufacturing variations proving key to composite behavior. While supplier specifications indicated uniform fiber dimensions (0.2–0.3 mm diameter, 10–60 mm length), measured AR displayed substantial batch-dependent deviations that directly influenced mechanical outcomes: the 0.5% RSF group (Batch A, Figure 7-a) exhibited extremely high AR (280–300), causing fiber clustering that reduced 28 day compressive strength to 29.76 MPa (33% below control) despite an assumed reinforcement potential. Optimal performance emerged in the 1.0% RSF formulation (Batch B, Figure 7-b), where tightly distributed AR (mean 80±5, mode 80) enabled homogeneous dispersion, achieving a peak compressive strength of 47.8 MPa alongside stable electro-resistive behavior under flexural loads. The higher 1.5% dosage (Batch C, Figure 7-c) contained shorter fibers (AR 50–60) which, somewhat unexpectedly, still enhanced compressive strength to 50.1 MPa, possibly via localized fiber network effects, although flexural capacity did not increase beyond that of Batch B. These results highlight the non-linear relationship between fiber dosage and composite performance, highlighting AR distribution as a dominant factor in fiber–matrix interaction efficiency. This finding validates the use of a fiber reinforcing index in our modeling, while emphasizing the necessity of manufacturing quality control to optimize fiber geometry for reliable structural performance.

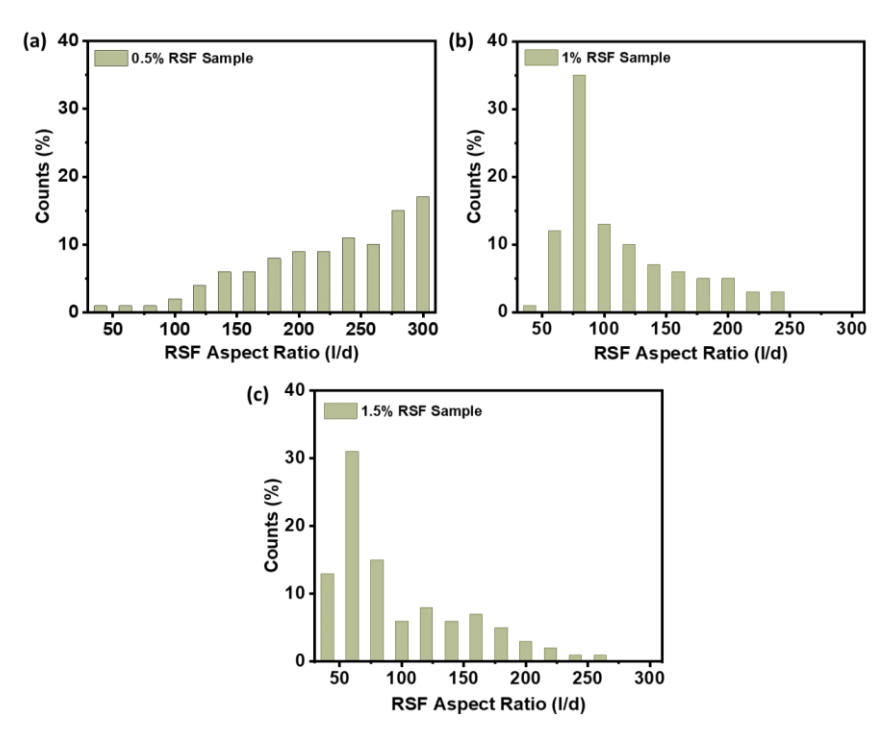


Figure 7. Aspect ratio distribution of RSF in various samples. (a) 0.5% RSF loaded sample; (b) 1% RSF loaded sample; (c) 1.5% RSF loaded sample

The SEM images in Figure 8 shows the microstructural changes and fiber-matrix interactions across mortar samples with different RSF contents. The SEM image of the control sample reveals the presence of voids and microcracks, as shown in Figure 8-a. The absence of fibers leads to unrestrained crack propagation and weak internal cohesion, which is consistent with the lowest mechanical strength and electrical conductivity observed. The 0.5% RSF sample exhibits poor fiber bonding with the surrounding mortar matrix. The fiber-matrix interface shows gaps and debonded regions, suggesting ineffective stress transfer and weak mechanical interlocking (see Figure 8-b). This correlates with the significantly reduced compressive strength for this sample. While in 1% RSF sample the microstructure shows wellintegrated fibers with the cement matrix (see Figure 8-c). The fibers appear fully embedded and tightly bonded to the surrounding mortar, indicating strong interfacial adhesion. This effective bonding enhances load transfer and crack bridging, supporting the highest mechanical performance and stable electrical response in this mix. In 1.5% RSF sample, with increase in fiber density, the SEM image reveals signs of bonding deterioration, as shown in Figure 8-d. In several areas, mortar detachment from the fiber periphery is visible, suggesting weak interfacial zones possibly caused by fiber clustering. This leads to localized stress concentrations and could explain the slight increase in compressive strength despite increased fiber content. These microstructural observations validate the mechanical and electrical conductivity trends across RSF-reinforced samples and highlight the importance of optimal fiber dispersion and bonding achieved most effectively at 1% RSF content.

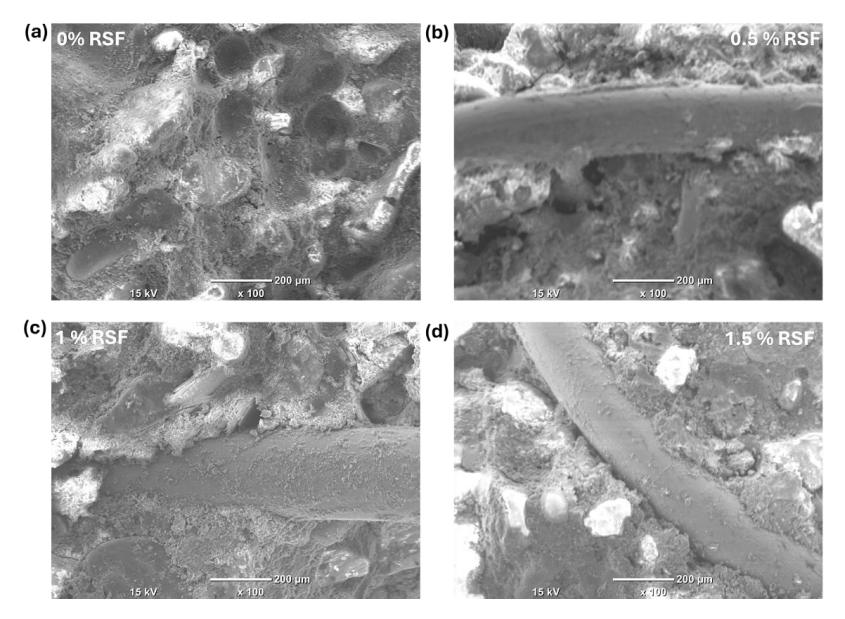


Figure 8. SEM image for 28-day cured sample (a) 0% RSF loaded sample; (b) 0.5% RSF loaded sample; (c) 1% RSF loaded sample; (d) 1.5% RSF loaded sample

#### 4. Conclusion

This study comprehensively demonstrated the dual benefits of incorporating recycled steel fibers (RSF) extracted from waste tires into cementitious composites, offering substantial mechanical enhancements, stable electrical properties, and significant sustainability advantages. Experimental results revealed that mortar specimens reinforced with 1% RSF achieved a 7.2% increase in compressive strength and a 26% improvement in flexural strength compared to the unreinforced control, highlighting the positive influence of appropriately dosed fiber reinforcement on mechanical performance. Increasing the RSF content to 1.5% resulted in a 12.6% gain in compressive strength relative to the control; however, this additional improvement was accompanied by a marginal decline in fiber dispersion efficiency and workability, suggesting diminishing returns beyond the 1% threshold. Electrical conductivity was notably enhanced across all RSF-modified mixes, with 0.5% RSF specimens demonstrating the lowest specific resistance due to the predominance of high-aspect-ratio fibers forming conductive pathways. Nevertheless, this increase in conductivity did not correlate with mechanical improvements, underscoring the critical importance of achieving balanced fiber dispersion rather than relying solely on fiber quantity or geometry.

The empirical models developed using the fiber reinforcing index ( $\xi$ ) effectively captured the observed strength trends, corroborating that an optimal combination of fiber volume fraction and aspect ratio is essential for maximizing structural benefits. Microstructural analysis further validated these findings, showing that 1% RSF samples exhibited superior fiber-matrix bonding with minimal voids, while 1.5% RSF mixes displayed localized bonding deterioration due to fiber clustering. Additionally, real-time monitoring of specific resistance during flexural loading revealed that the resistance slope strongly correlated with damage evolution, confirming the potential for integrating structural health monitoring (SHM) capabilities into RSF-reinforced composites. Future studies will also explore the repeatability of the electrical sensing response under cyclic loading to further validate the long-term SHM capabilities of RSF-reinforced composites. Furthermore, the integration of a fiber-reinforcing index-based strength model with in-situ electrical resistance monitoring in this study represents a novel methodology, providing a foundation for future development of smart, self-monitoring fiber-reinforced composites. Collectively, these results affirm that the optimal incorporation of RSF, particularly at a 1% volume fraction, offers a cost-effective, sustainable, and technically viable alternative to virgin industrial fibers, advancing the development of smart, eco-friendly construction materials aligned with modern sustainability and infrastructure resilience goals. These findings highlight the broader significance of using waste-derived fibers to engineer high-performance, self-monitoring construction materials. Such an approach effectively translates a local waste management challenge into a globally applicable solution for sustainable infrastructure.

#### 5. Declarations

### 5.1. Author Contributions

Conceptualization, U.A. and M.R.A.R.I.; methodology, U.A., M.R.A.R.I., N.A., H.Y.K., and K.K.; formal analysis, U.A., M.R.M., N.A., and R.K.R.; data curation, U.A.; writing—original draft preparation, U.A. and M.R.A.R.I.; writing—review and editing, M.R.M., R.K.R., and K.K. All authors have read and agreed to the published version of the manuscript.

## 5.2. Data Availability Statement

The data presented in this study are available on request from the corresponding author.

#### 5.3. Funding and Acknowledgements

This work was supported by Qatar University under high-impact grant # QUHI-CAM-24/25-518 and we are also thankful to Engr. Mohammed Matar, General Manager at Bright Future Tyre Recycling Factory, Qatar for recycled steel fibers. The authors acknowledge the use of Grammarly (Grammarly Inc., 2024) for grammar checking, spell-checking, and language enhancement to improve the clarity and readability of this manuscript. All scientific content, research methodology, data analysis, interpretation, and conclusions remain entirely the work of the authors. The authors take full responsibility for the accuracy and integrity of all content presented in this manuscript.

#### 5.4. Conflicts of Interest

The authors declare no conflict of interest.

#### 6. References

- [1] Liu, G., Claramunt, J., Hunger, M., Tošić, N., & de la Fuente, A. (2024). Effect of coarse recycled aggregate with embedded fibres on the mechanical properties and microstructure of polypropylene fibre-reinforced concrete. Materials and Structures, 57(10), 241. doi:10.1617/s11527-024-02527-3.
- [2] Chakraborty, S., & Subramaniam, K. V. L. (2023). Evaluation of cracking and cohesive fracture response in recycled aggregate concrete. Materials and Structures, 56(7), 130. doi:10.1617/s11527-023-02193-x.

[3] Anike, E. E., Saidani, M., Ganjian, E., Tyrer, M., & Olubanwo, A. O. (2020). Evaluation of conventional and equivalent mortar volume mix design methods for recycled aggregate concrete. Materials and Structures, 53(1), 22. doi:10.1617/s11527-020-1457-3.

- [4] Marzouk, O. Y., Dheilly, R. M., & Queneudec, M. (2007). Valorization of post-consumer waste plastic in cementitious concrete composites. Waste Management, 27(2), 310–318. doi:10.1016/j.wasman.2006.03.012.
- [5] Zhao, Z., Xiao, F., & Amirkhanian, S. (2020). Recent applications of waste solid materials in pavement engineering. Waste Management, 108, 78–105. doi:10.1016/j.wasman.2020.04.024.
- [6] Bahij, S., Omary, S., Feugeas, F., & Faqiri, A. (2020). Fresh and hardened properties of concrete containing different forms of plastic waste A review. Waste Management, 113, 157–175. doi:10.1016/j.wasman.2020.05.048.
- [7] Onuaguluchi, O., & Banthia, N. (2018). Scrap tire steel fiber as a substitute for commercial steel fiber in cement mortar: Engineering properties and cost-benefit analyses. Resources, Conservation and Recycling, 134, 248–256. doi:10.1016/j.resconrec.2018.03.014.
- [8] Abdolpour, H., Niewiadomski, P., Sadowski, Ł., & Kwiecień, A. (2022). Engineering of ultra-high performance self-compacting mortar with recycled steel fibres extracted from waste tires. Archives of Civil and Mechanical Engineering, 22(4), 175. doi:10.1007/s43452-022-00496-4.
- [9] Belli, A., Mobili, A., Bellezze, T., & Tittarelli, F. (2020). Commercial and recycled carbon/steel fibers for fiber-reinforced cement mortars with high electrical conductivity. Cement and Concrete Composites, 109, 103569. doi:10.1016/j.cemconcomp.2020.103569.
- [10] Domski, J., Katzer, J., Zakrzewski, M., & Ponikiewski, T. (2017). Comparison of the mechanical characteristics of engineered and waste steel fiber used as reinforcement for concrete. Journal of Cleaner Production, 158, 18–28. doi:10.1016/j.jclepro.2017.04.165.
- [11] Carrillo, J., Lizarazo-Marriaga, J., & Lamus, F. (2020). Properties of Steel Fiber Reinforced Concrete Using Either Industrial or Recycled Fibers from Waste Tires. Fibers and Polymers, 21(9), 2055–2067. doi:10.1007/s12221-020-1076-1.
- [12] Aiello, M. A., Leuzzi, F., Centonze, G., & Maffezzoli, A. (2009). Use of steel fibres recovered from waste tyres as reinforcement in concrete: Pull-out behaviour, compressive and flexural strength. Waste Management, 29(6), 1960–1970. doi:10.1016/j.wasman.2008.12.002.
- [13] Centonze, G., Leone, M., & Aiello, M. A. (2012). Steel fibers from waste tires as reinforcement in concrete: A mechanical characterization. Construction and Building Materials, 36, 46–57. doi:10.1016/j.conbuildmat.2012.04.088.
- [14] Liew, K. M., & Akbar, A. (2020). The recent progress of recycled steel fiber reinforced concrete. Construction and Building Materials, 232, 117232. doi:10.1016/j.conbuildmat.2019.117232.
- [15] Zia, A., Pu, Z., Holly, I., Umar, T., Tariq, M. A. U. R., & Sufian, M. (2022). A Comprehensive Review of Incorporating Steel Fibers of Waste Tires in Cement Composites and Its Applications. Materials, 15(21), 7420. doi:10.3390/ma15217420.
- [16] Zhang, P., Wang, C., Wu, C., Guo, Y., Li, Y., & Guo, J. (2022). A review on the properties of concrete reinforced with recycled steel fiber from waste tires. Reviews on Advanced Materials Science, 61(1), 276–291. doi:10.1515/rams-2022-0029.
- [17] Barros, J. A. O., Frazão, C., Caggiano, A., Folino, P., Martinelli, E., Xargay, H., Zamanzadeh, Z., & Lourenço, L. (2017). Cementitious Composites Reinforced with Recycled Fibres. Recent Advances on Green Concrete for Structural Purposes. Research for Development. Springer, Cham, Switzerland. doi:10.1007/978-3-319-56797-6\_8.
- [18] Amin, M. N., Khan, K., Nazar, S., & Deifalla, A. F. (2023). Application of waste recycle tire steel fibers as a construction material in concrete. Reviews on Advanced Materials Science, 62(1), 20220319. doi:10.1515/rams-2022-0319.
- [19] Alsaif, A., & Alharbi, Y. R. (2022). Strength, durability and shrinkage behaviours of steel fiber reinforced rubberized concrete. Construction and Building Materials, 345, 128295. doi:10.1016/j.conbuildmat.2022.128295.
- [20] Mehmandari, T. A., Shokouhian, M., Imani, M., Tee, K. F., & Fahimifar, A. (2025). Split Tensile Behavior of Recycled Steel Fiber-Reinforced Concrete. ACI Materials Journal, 122(2), 15–28. doi:10.14359/51744375.
- [21] Meddah, M. S., & Bencheikh, M. (2009). Properties of concrete reinforced with different kinds of industrial waste fibre materials. Construction and Building Materials, 23(10), 3196–3205. doi:10.1016/j.conbuildmat.2009.06.017.
- [22] Samarakoon, S. M. S. M. K., Ruben, P., Wie Pedersen, J., & Evangelista, L. (2019). Mechanical performance of concrete made of steel fibers from tire waste. Case Studies in Construction Materials, 11, 259. doi:10.1016/j.cscm.2019.e00259.
- [23] Balaguru, P., & Najm, H. (2004). High-performance fiber-reinforced concrete mixture proportions with high fiber volume fractions. Materials Journal, 101(4), 281-286. doi:10.14359/13361.
- [24] Khalel, H. H. Z., Khan, M., Starr, A., Sadawi, N., Mohamed, O. A., Khalil, A., & Esaker, M. (2025). Parametric study for optimizing fiber-reinforced concrete properties. Structural Concrete, 26(1), 88–110. doi:10.1002/suco.202300509.

[25] Soltanzadeh, F., Behbahani, A. E., Hosseinmostofi, K., & Teixeira, C. A. (2022). Assessment of the Sustainability of Fibre-Reinforced Concrete by Considering Both Environmental and Mechanical Properties. Sustainability (Switzerland), 14(10), 6347. doi:10.3390/su14106347.

- [26] Soulioti, D. V., Barkoula, N. M., Paipetis, A., & Matikas, T. E. (2011). Effects of Fibre Geometry and Volume Fraction on the Flexural Behaviour of Steel- Fibre Reinforced Concrete. Strain, 47, e535-e541. doi:10.1111/j.1475-1305.2009.00652.x.
- [27] Centonze, G., Leone, M., Micelli, F., Colonna, D., & Aiello, M. A. (2016). Concrete reinforced with recycled steel fibers from end of life tires: Mix-design and application. Key Engineering Materials, 711, 224-231. doi:10.4028/www.scientific.net/KEM.711.224.
- [28] Papakonstantinou, C. G., & Tobolski, M. J. (2006). Use of waste tire steel beads in Portland cement concrete. Cement and Concrete Research, 36(9), 1686–1691. doi:10.1016/j.cemconres.2006.05.015.
- [29] Zeybek, Ö., Özkılıç, Y. O., Çelik, A. İ., Deifalla, A. F., Ahmad, M., & Sabri Sabri, M. M. (2022). Performance evaluation of fiber-reinforced concrete produced with steel fibers extracted from waste tire. Frontiers in Materials, 9. doi:10.3389/fmats.2022.1057128.
- [30] Chen, M., Si, H., Fan, X., Xuan, Y., & Zhang, M. (2022). Dynamic compressive behaviour of recycled tyre steel fibre reinforced concrete. Construction and Building Materials, 316, 125896. doi:10.1016/j.conbuildmat.2021.125896.
- [31] Frazão, C. M. V., Barros, J. A. B., & Bogas, J. A. (2019). Durability of recycled steel fiber reinforced concrete in chloride environment. Fibers, 7(12), 111. doi:10.3390/fib7120111.
- [32] Revuelta, D., Carballosa, P., García Calvo, J. L., & Pedrosa, F. (2021). Residual strength and drying behavior of concrete reinforced with recycled steel fiber from tires. Materials, 14(20), 6111. doi:10.3390/ma14206111.
- [33] Qin, X., & Kaewunruen, S. (2022). Environment-friendly recycled steel fibre reinforced concrete. Construction and Building Materials, 327, 126967. doi:10.1016/j.conbuildmat.2022.126967.
- [34] Li, G., Garrick, G., Eggers, J., Abadie, C., Stubblefield, M. A., & Pang, S. S. (2004). Waste tire fiber modified concrete. Composites Part B: Engineering, 35(4), 305–312. doi:10.1016/j.compositesb.2004.01.002.
- [35] Mastali, M., & Dalvand, A. (2017). Fresh and Hardened Properties of Self-Compacting Concrete Reinforced with Hybrid Recycled Steel-Polypropylene Fiber. Journal of Materials in Civil Engineering, 29(6), 04017012. doi:10.1061/(asce)mt.1943-5533.0001851.
- [36] Martinelli, E., Caggiano, A., & Xargay, H. (2015). An experimental study on the post-cracking behaviour of Hybrid Industrial/Recycled Steel Fibre-Reinforced Concrete. Construction and Building Materials, 94, 290–298. doi:10.1016/j.conbuildmat.2015.07.007.
- [37] Pilakoutas, K., Neocleous, K., & Tlemat, H. (2004). Reuse of tyre steel fibres as concrete reinforcement. Engineering Sustainability, 157(3), 131–138. doi:10.1680/ensu.157.3.131.48644.
- [38] Albano, C., Camacho, N., Reyes, J., Feliu, J. L., & Hernández, M. (2005). Influence of scrap rubber addition to Portland I concrete composites: Destructive and non-destructive testing. Composite Structures, 71(3–4), 439–446. doi:10.1016/j.compstruct.2005.09.037.
- [39] Rashid, K., & Balouch, N. (2017). Influence of steel fibers extracted from waste tires on shear behavior of reinforced concrete beams. Structural Concrete, 18(4), 589–596. doi:10.1002/suco.201600194.
- [40] Caggiano, A., Gambarelli, S., Martinelli, E., Nisticò, N., & Pepe, M. (2016). Experimental characterization of the post-cracking response in Hybrid Steel/Polypropylene Fiber-Reinforced Concrete. Construction and Building Materials, 125, 1035–1043. doi:10.1016/j.conbuildmat.2016.08.068.
- [41] Majeed Abed, Z., Khalil, W. I., & Ahmed, H. K. (2024). Tire wastes and durability: the influence of crumb rubber and recycled steel fibre on properties of roller compacted concrete. International Journal of Pavement Engineering, 25(1), 2372628. doi:10.1080/10298436.2024.2372628.
- [42] Romero, A. J., & Moustafa, M. A. (2025). Effect of recycled tires steel fibers characteristics on crack behavior and mechanical properties of scalable ultra-economical UHPC. Journal of Building Engineering, 99, 111582. doi:10.1016/j.jobe.2024.111582.
- [43] Abdulkarim, A., Riahi, H. T., & Ataei, A. (2025). Comparative study of mechanical properties of one-part alkali-activated slag concrete using deformed and recycled tire steel fibers. Case Studies in Construction Materials, 22, 4124. doi:10.1016/j.cscm.2024.e04124.
- [44] Doğruyol, M., Ayhan, E., & Karaşin, A. (2024). Effect of waste steel fiber use on concrete behavior at high temperature. Case Studies in Construction Materials, 20, 3051. doi:10.1016/j.cscm.2024.e03051.
- [45] Frazão, C., Barros, J., Bogas, J. A., García-Cortés, V., & Valente, T. (2022). Technical and environmental potentialities of recycled steel fiber reinforced concrete for structural applications. Journal of Building Engineering, 45, 103579. doi:10.1016/j.jobe.2021.103579.

[46] Mastali, M., & Dalvand, A. (2016). Use of silica fume and recycled steel fibers in self-compacting concrete (SCC). Construction and Building Materials, 125, 196–209. doi:10.1016/j.conbuildmat.2016.08.046.

- [47] Aïtcin, P.-C. (2016). The importance of the water–cement and water–binder ratios. Science and Technology of Concrete Admixtures, 3–13, Woodhead Publishing, Sawston, United Kingdom. doi:10.1016/b978-0-08-100693-1.00001-1.
- [48] Shi, X., Brescia-Norambuena, L., Grasley, Z., & Hogancamp, J. (2020). Fracture Properties and Restrained Shrinkage Cracking Resistance of Cement Mortar Reinforced by Recycled Steel Fiber from Scrap Tires. Transportation Research Record, 2674(8), 581–590. doi:10.1177/0361198120924407.
- [49] ASTM C305-13. (2014). Standard Practice for Mechanical Mixing of Hydraulic Cement Pastes and Mortars of Plastic Consistency. ASTM International, Pennsylvania, United States. doi:10.1520/C0305-13
- [50] ASTM C109/C109M-20b. (2021). Standard Test Method for Compressive Strength of Hydraulic Cement Mortars (Using 2-in. or [50 mm] Cube Specimens). ASTM International, Pennsylvania, United States. doi:10.1520/C0109\_C0109M-20B.
- [51] ASTM C348-21. (2021). Standard Test Method for Flexural Strength of Hydraulic-Cement Mortars. ASTM International, Pennsylvania, United States. doi:10.1520/C0348-21.
- [52] ASTM C150/C150M-22. (2024). Standard Specification for Portland Cement. ASTM International, Pennsylvania, United States. doi:10.1520/C0150\_C0150M-22.
- [53] ASTM C778-13. (2017). Standard Specification for Standard Sand. ASTM International, Pennsylvania, United States. doi:10.1520/C0778-13.
- [54] Turk, K., Cicek, N., Katlav, M., Donmez, I., & Turgut, P. (2023). Electrical conductivity and heating performance of hybrid steel fiber-reinforced SCC: The role of high-volume fiber and micro fiber length. Journal of Building Engineering, 76, 107392. doi:10.1016/j.jobe.2023.107392.
- [55] Wen, S., & Chung, D. D. L. (2007). Double percolation in the electrical conduction in carbon fiber reinforced cement-based materials. Carbon, 45(2), 263–267. doi:10.1016/j.carbon.2006.09.031.
- [56] Ou, Y.-C., Tsai, M.-S., Liu, K.-Y., & Chang, K.-C. (2012). Compressive Behavior of Steel-Fiber-Reinforced Concrete with a High Reinforcing Index. Journal of Materials in Civil Engineering, 24(2), 207–215. doi:10.1061/(asce)mt.1943-5533.0000372.
- [57] Nzambi, A. K. L. L., Ntuku, J. B., & de Oliveira, D. R. C. (2022). Empirical equations for flexural residual strengths in concrete with low volumetric fractions of hook-end steel fiber. Engineering Reports, 4(5), e12490. doi:10.1002/eng2.12490.
- [58] Leone, M., Centonze, G., Colonna, D., Micelli, F., & Aiello, M. A. (2016). Experimental Study on Bond Behavior in Fiber-Reinforced Concrete with Low Content of Recycled Steel Fiber. Journal of Materials in Civil Engineering, 28(9), 04016068. doi:10.1061/(asce)mt.1943-5533.0001534.
- [59] Skarżyński, Ł., & Suchorzewski, J. (2018). Mechanical and fracture properties of concrete reinforced with recycled and industrial steel fibers using Digital Image Correlation technique and X-ray micro computed tomography. Construction and Building Materials, 183, 283–299. doi:10.1016/j.conbuildmat.2018.06.182.